CREEP PROPERTIES AND PREDICTION MODEL OF PADDY SOIL UNDER COMPRESSION
/
水稻土受压蠕变特性及预测模型构建

Guoyang Liu[1)], Junfang Xia[1,2)], Kan Zheng*[1,2)], Jian Cheng[1)], Liu Jiang[1)], Liwei Guo[1)]
[1)] College of Engineering, Huazhong Agricultural University, Wuhan 430070 / China
[2)] Key Laboratory of Agricultural Equipment in Mid-lower Reaches of Yangtze River, Ministry of Agriculture and Rural Affairs, Wuhan 430070 / China
Tel: +86 15271890761; E-mail: zhengkan@mail.hzau.edu.cn
DOI: https://doi.org/10.356.33/inmateh-65-46

Keywords: *constitutive equation; stress level; creep model; viscoplasticity; strain; paddy soil*

ABSTRACT
In order to study the compressive creep properties and laws of paddy soil, multi-stress creep experiments of paddy soil with different moisture content were carried out. The results show that the creep deformation of paddy soil, subjected to compressive loads effect, develops stably and the paddy soil is not destructed under the yield strength when the stress is low. When the stress level is higher than the yield strength, the internal damage of paddy soil would be caused at the moment of loading. With the extension of creep time, the cracks would gradually expand, resulting in the soil to yield, break and disintegrate. According to the analysis of the deformation properties of paddy soil under compression and the change trend of creep curve, the nonlinear viscoelastic-plastic model was composed of the nonlinear viscoplastic model and Burgers model in series. The creep test curve was introduced into the model for fitting, and the coefficient of determination reached more than 0.96. Based on the model, the strain composition, strain proportion, and strain rate of paddy soil were studied. Finally, the nonlinear model was compared with Burgers model by verification test. The fitting accuracy of the nonlinear model was better than Burgers model, and the coefficient of determination and relative error were 0.997 and 0.437%, respectively, which proved the rationality and correctness of the nonlinear viscoelastic-plastic model. This study can provide a theoretical basis for the optimization of tillage machinery structure and the simulation analysis of soil tillage and compaction.

摘要
为研究水稻土受压蠕变性能，探究其蠕变规律，以不同含水率的水稻土为试验对象进行多应力蠕变试验。试验结果表明水稻土在持续受压载荷作用下，应力水平较低时，蠕变变形发展稳定，不会发生失效破坏；应力水平大于屈服强度时，加载瞬间就会导致土壤内部损伤，随着蠕变时间延长，裂纹逐渐扩展致使土壤受压屈服破坏解体。通过分析水稻土受压变形特征和蠕变曲线变化趋势，将非线性黏塑性模型与 Burgers 模型串联组成非线性黏弹塑性模型，并将蠕变试验曲线引入该模型进行拟合，决定系数均达到 0.96 以上。基于推导的模型探究了水稻土受压蠕变各应变组成、应变占比以及应变速率规律，最后通过验证试验将该非线性模型与 Burgers 模型进行对比，结果表明非线性模型拟合精度优于 Burgers 模型，其决定系数和相对误差分别为 0.997、0.437%，证实了所建立的非线性黏弹塑性模型的合理性与正确性。本研究可为耕作机械结构优化及土壤耕作、压实等相关仿真分析提供理论依据。

INTRODUCTION
Soil is the main operation object for tillage machinery (*Romaneckas, & Jasinskas, 2017*). Due to the complexity of soil physical composition (*Schmalz et al., 2013*), dynamic factors of tillage machinery (*Zeng, Chen, & Zhang, 2017*), and adhesion of soil particles (*Wang et al., 2019*), the tillage process is very complicated. As a kind of complex rheological body, soil rheology presents the properties of deformation and flow under the action of external force. Therefore, soil rheology is essential in the research and development of tillage machinery and formulation of agronomy. The results of such can provide some new ideas for optimal design of tillage machinery with the aim to reduce resistance and traction performance improvement.

[1] *Guoyang Liu, Ph.D. Stud. Eng.; Junfang Xia, Prof. Ph.D.; Kang Zheng, Lec. Ph.D. Eng.; Jian Cheng, M.S. Stud. Eng.; Liu Jiang, M.S. Stud. Eng.; Liwei Guo, M.S. Stud. Eng.*

Creep model plays an important role in the theoretical research of rheological mechanics properties, which can be used to accurately reflect and predict the rheology of materials. For example, *Kong et al.* studied the mechanical properties of seed cotton compression and stress relaxation process and constructed its constitutive model. This finding can provide a profound theoretical basis to simulate seed cotton compression in most cotton picking areas (*Kong et al., 2021*). It has been proposed that both temperature and moisture content affect the tensile creep and recovery by influencing the formation and fracture of hydrogen bonds according to Norway spruce creep tests (*Engelund and Salmen, 2012*). In addition to using creep model to characterize the mechanical properties of materials, researchers have also developed creep model to make it suitable for the prediction and evaluation of material rheology in multiple environments. Combing the test results of creep deformation properties of frozen soil with the theory of binary medium model, *Wang et al.* analysed the creep fracture mechanism of frozen soil in detail and proposed a new binary medium creep constitutive model (*Wang et al., 2021*). Meanwhile, a new fractional creep model of soft soil was established by introducing Almeida fractional derivative into the classical elastic-viscoplastic model. The fractional creep model required fewer material parameters and state variables than the traditional model. It exhibited higher accuracy and convenience (*Xiang et al., 2021*).

The soil in the middle and lower of the Yangtze River, alternates between dry and wet all year round, resulting in soil sticking and hardening. The physical state of soil was related to the form of soil deformation during cultivating in the field (*Zheng et al., 2019; Zhu et al., 2020*). From the perspective of soil deformation, the soil with strong viscoplasticity could withstand large plastic deformation without little fracture and fragmentation. When tillage machinery was working in such paddy fields, the straw burial rate and surface flatness would be decreased (*Zhu et al., 2019*). Therefore, how to accurately predict and evaluate the rheology and creep process of the soil has become a research point of agricultural machinery.

In this study, we carried out compression creep tests on paddy soil with different moisture content in multi stress load. The nonlinear viscoelastic-plastic creep model was established based on creep test curves, and creep model parameters and deformation laws were obtained. It is expected to provide a theoretical basis for the research on high efficiency and low consumption design of agricultural equipment, related simulation parameter selection of tillage machinery.

MATERIALS AND METHODS

Experimental materials

The soil used in the experiment was taken from the paddy field in the Modern Agricultural Science and Technology Experimental Base of Huazhong Agricultural University (30°28′N, 114°21′E). The annual double-crop rotation system (rice - wheat and rice - rape) is the domain planting pattern. During the experiment, the surface rice stubble and weeds in the sampling area were removed, and the soil of tillage layer was collected by five point sampling method. The soil moisture content is 27.16%; the dry density is 1.48 g/cm^3; the organic matter content is 20.31 g/kg, and the mass fractions of clay (< 0.002 mm), powder (0.002-0.05 mm) and sand (0.05-2.0 mm) are 41.36%, 50.73% and 7.91% respectively.

The above experimental field was sampled again at an interval of 30 days, and the measured moisture content of the second sampling soil was 21.51%. Soil samples were collected to conduct creep test by a cylindrical ring knife with a diameter of 70 mm and a height of 52 mm. We took the average compressive strength obtained from the same batch of soil compression test as the stress reference value of creep test, and regarded 15%, 30%, 45%, 60% and 75% of compressive strength as the stress level. In order to conveniently describe the experiment process and results, the above two soils were called w_1 and w_2 soil respectively. We numbered it *w*1015 - *w*2075 according to the stress level.

Table 1

Numbers of soil creep samples under compression

Moisture content [%]	27.61					21.51				
Number	*w*1015	*w*1030	*w*1045	*w*1060	*w*1075	*w*2015	*w*2030	*w*2045	*w*2060	*w*2075
Stress level [%]	15	30	45	60	75	15	30	45	60	75
Stress [MPa]	0.016	0.032	0.048	0.064	0.080	0.017	0.034	0.051	0.068	0.085

Experimental methods

The TMS-PRO texture analyser (American FTC company) was used as the creep test equipment, which could provide a maximum test force of 1000 N and accuracy of ±1% (Fig. 1). A disk-shaped probe with the diameter of 75 mm was selected to conduct compression creep tests. The sample was placed and fixed on the test bench. After setting predetermined load, the disk moved downward at the velocity of 20 mm/min. When reaching the predetermined load, the pressure was maintained for 900 s. When the pressure holding time was over, the disk returned automatically. The force, displacement and time during the experiment were automatically recorded and saved with sampling frequency of 50 Hz. The soil strain was the ratio of the displacement difference collected by the sensor to the soil initial height (52 mm).

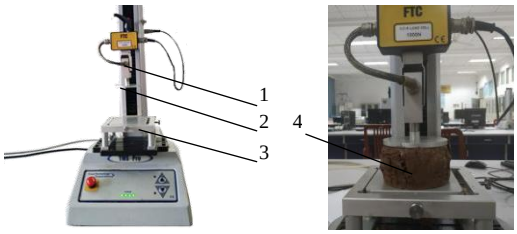

Fig. 1 - Creep test bench

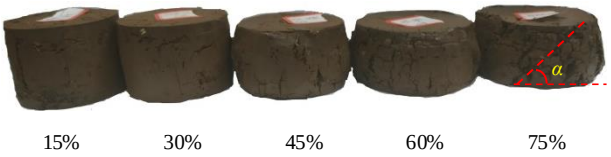

Fig. 2 - Creep failure of soil under compression

1– sensor; 2 – disc indenter; 3 – support; 4 – soil sample

RESULTS AND DISCUSSIONS

Soil compression creep properties

After the soil was removed from the test bench, the soil strain recovered slightly. With the extension of time, the greater the recovery value of strain was, the smaller the recovery speed was (Fig. 2). However, there was still permanent deformation of soil after long-time recovery, and it could not return to the initial state before loading. The final shape was waist drum shape, and the increase of applied stress had positive effect on the creep deformation. When the stress of soil was between elastic strength and yield strength, the soil would produce elastic deformation. Creep deformation gradually increased with the increase of creep time. Therefore, the soil with 15% and 30% stress levels only deformed in the whole creep process, and there was no crack on the surface. Because the applied stress was close to the yield strength of the soil, there was deformation and surface cracks of the samples with 45% and 60% stress levels in the creep process. The waist drum position of these samples deviated from the centre and was close to the bottom. Although the soil sample had cracks, it did not disintegrate. The waist drum shape of the sample at 75% stress level was located in the top. The appearance of the sample looked rough with destructive soil particles protruding from its surface. The reason was that the soil was an anisotropic material with inconsistent internal strength. If a certain position of soil reached the yield strength, the cracks would occur. With the increase of creep time, the internal damage gradually accumulated, and finally the internal and external cracks penetrated to form macro cracks. Moreover, the soil was destroyed under plastic deformation, and the angle between the soil failure section and the horizontal plane α was about 45°. It showed that the soil firstly reached the shear stress strength and then was damaged.

In order to study the law of soil compression creep deformation under different stress levels, taking the instantaneous strain of reaching the predetermined load as the starting point, we calculated the growth rate (ζ_t) of each time relative to this point in the pressure holding time. The calculation formula was as follows:

$$\zeta_t = \frac{\varepsilon_t - \varepsilon_0}{\varepsilon_0} \times 100\% \quad (1)$$

Where, ζ_t is the growth rate of strain at time t, %; ε_t is the strain at time t, %; ε_0 is the instantaneous strain, %.

As shown in Fig. 3, the initial instantaneous strain and final steady state strain increased with the increase of stress level, and the creep curve was consistent and similar. All the samples produced instantaneous strain during loading. Because the loading time was shorter than the later creep time, it could be considered that the elastic deformation occurred instantaneously. After elastic deformation, the strain of the soil initially increased linearly with the increase of creep time, and then the creep rate decreased gradually. The overall creep curve showed nonlinear characteristics. Although the creep strain at 15% and 30% stress levels increased with time, the creep rate almost approached 0 at the later stage of creep. The soil strain at 45% and 60% stress levels changed more obviously with time. In the later stage of creep, the strain increased approximately linearly with time, and the creep deformation rate was high.

The creep curve was steeper than that at low stress level. For soils subjected to 75% stress level, the strain and strain rate increase rapidly after compression, and the value was higher than that of other stress levels.

Since the stress of the soil under 75% stress level exceeded its yield strength, the time to reach creep failure in the pressure holding process was shorter. The strain rate of the soil was faster and its growth rate was greater than 1, so the strain growth rate curve at 75% stress level was not drawn in Fig. 3. The strain growth rate of each sample increased with the increasing time, and the strain growth rate decreased gradually. Generally speaking, the strain growth rate of two groups of soil samples with different moisture content initially increased rapidly, and gradually increased slowly after 100 s. The nonlinear relationship was more and more obvious, showing the stages of instantaneous creep and attenuation creep.

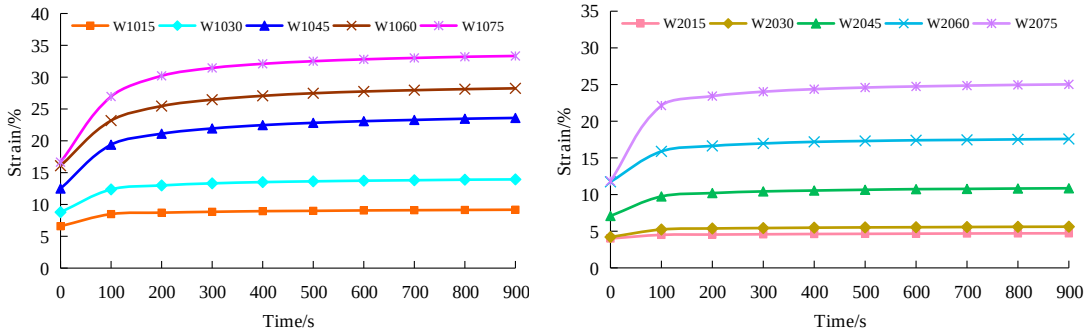

(a) The curve of relationship between time and strain

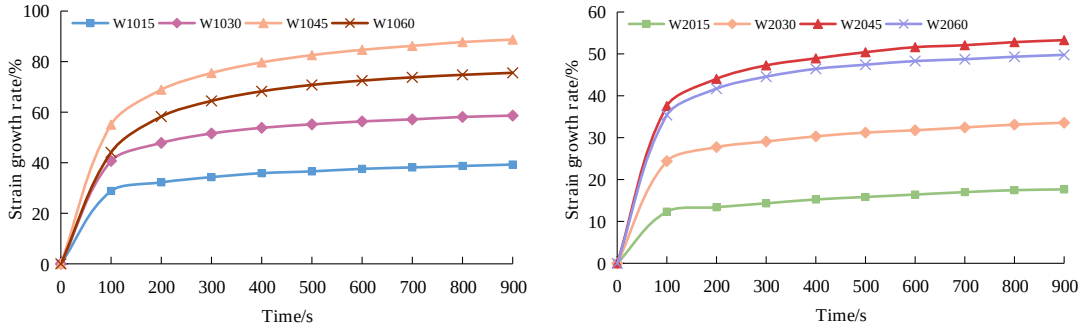

(b) The curve of relationship between time and strain growth rate curve

Fig. 3 - Creep characteristic curve of soil under different stress levels

For the initial strain, steady state strain and strain rate of the sample, the change trend of the two groups of soil with different moisture content was the same, which increased with the increase of stress level (Table 2). However, the final strain growth rate of 60% stress level was lower than that of 45% stress level in two sets of test samples. It may be that the applied stress of 60% stress level was high, which could destroy some fragile areas in the soil interior. The force applied during the pressure holding process could gather and compact the evacuated soil particles, resulting in the increase of deformation resistance and the decrease of deformation. After the stress level was greater than 30%, the trend of steady state strain was non convergent continuous growth. In addition, the strain growth rate of soils at 60% and 75% levels was also the trend until soil failure.

Table 2

Creep strain and strain growth rate of soil

Number	Initial strain [%]	Steady state strain [%]	Final strain growth rate [%]
*w*1015	6.59	9.18	39.29
*w*1030	8.79	13.94	58.64
*w*1045	12.50	23.59	88.71
*w*1060	16.09	28.24	75.57
*w*1075	16.65	33.33	/
*w*2015	4.01	4.72	17.65
*w*2030	4.21	5.62	33.56
*w*2045	7.08	10.86	53.28
*w*2060	11.74	17.58	49.76
*w*2075	11.85	25.03	/

Construction of nonlinear viscoelastic plastic creep model

From the above analysis, it could be seen that the deformation of soil under different stresses was also different. In order to establish the creep constitutive equation of paddy soil under multi stress environment, it was necessary to further analyse the deformation process and properties of soil. On the one hand, from the perspective of relationship between time and strain, the deformation increased rapidly in the initial stage of loading, and tended to be stable. After unloading, the soil rebounded slightly, but there was still residual deformation. On the other hand, from the perspective of relationship between time and strain rate, the strain rate decreased gradually with time and tended to 0. These results showed that the paddy soil conformed to the loading and unloading laws of viscoelastic materials and viscoplastic materials. Therefore, paddy soil could be regarded as a viscoelastic-plastic material. In addition to a single elastic, viscous and plastic strain, there are also complex coupling strains in the deformation process, such as viscoplastic and elastic-plastic strain. For such materials, it was difficult to accurately describe their nonlinear creep properties by traditional Kelvin, Maxwell and other models (*Aleksandar et al., 2020; Zou et al., 2013*).

Burgers model (Fig. 4a) was one of the common linear models, which could well describe the properties of soil instantaneous elastic deformation, delayed elastic deformation and viscous flow. However, when the creep time exceeded a certain time, the viscoelastic strain contributed by Maxwell model in the model had reached the maximum. Since then, the strain increment only came from viscous strain, which led to the linear growth trend of the predicted creep curve in the later stage. The phenomenon deviated from the objective fact that the creep curve tended to be stable (*Tia et al., 2009*). Therefore, such a linear model could not characterize the plastic deformation of soil. This kind of linear model could only meet the fitting requirements, and could not theoretically analyse the influence of multi stress load on soil creep deformation, which was not convenient for its application in numerical simulation.

Nonlinear viscoelastic-plastic creep model

Based on the experimental curve, a two-element nonlinear viscoplastic model composed of nonlinear damper and friction block was established (Fig. 4b). The soil compression creep curve was fitted by the correction method that the viscosity coefficient changed according to the law of power function, and the equation was:

$$\varepsilon = \varepsilon_0 + kt^n \tag{2}$$

When $\sigma > \sigma_s$, the two-element nonlinear viscoplastic creep model was triggered, and the relationship between strain and time was shown in equation (3). Combining equation (2) with equation (3), we defined $(\sigma - \sigma_s) / \eta_0 = k$. The expression of nonlinear damper η_s could be obtained:

$$\varepsilon = \varepsilon_0 + \frac{\sigma - \sigma_s}{\eta} t \tag{3}$$

$$\eta(\eta, t) = \eta_0 \frac{t_0^{n-1}}{t^{n-1}} = \frac{\eta_0}{t^{n-1}} \tag{4}$$

where, t_0 is the reference time, 1; η_0 is the initial viscosity coefficient, MPa·s; σ is the applied stress, MPa;

σ_s is the yield strength, MPa.

According to the above derivation process, the creep constitutive equation of the nonlinear viscoplastic model could be obtained.

$$\varepsilon(t) = \frac{H(\sigma - \sigma_s)}{\eta_{(n,t)}} t = \frac{H(\sigma - \sigma_s)}{\eta_{(n,t)}} t^n = = \begin{cases} 0 & (\sigma \le \sigma_s) \\ \dfrac{\sigma - \sigma_s}{\eta_{(n,t)}} t^n & (\sigma > \sigma_s) \end{cases} \tag{5}$$

Nonlinear viscoelastic-plastic creep model

Considering the complexity of soil compression deformation, the Burgers model was modified in this study. The nonlinear viscoplastic model was connected with it to form the six-element nonlinear viscoelastic-plastic creep model of soil (Fig. 4c). When the model was subjected to constant stress σ that was less than the soil yield strength, the six-element nonlinear viscoelastic-plastic creep model would degenerate into a four-element Burgers model. When the soil was subjected to constant stress σ that was greater than the soil yield strength, the nonlinear viscoplastic model was triggered. The model stress passed through the friction block σ_s was attenuated and transferred to Burgers model.

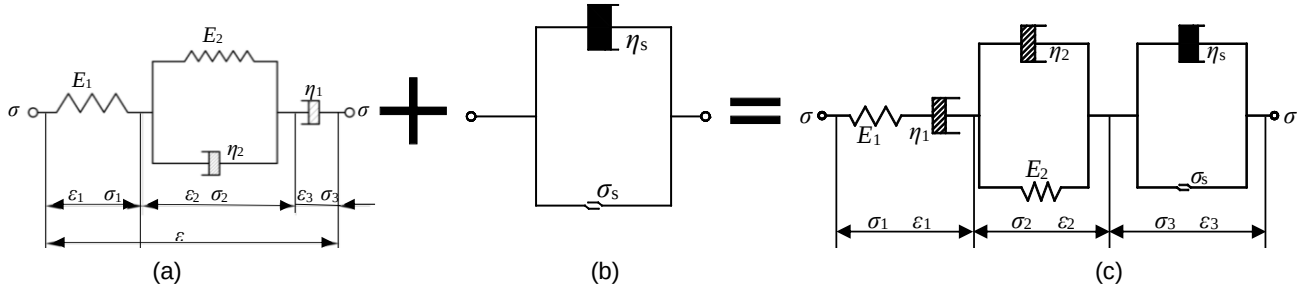

Fig. 4 - Nonlinear viscoelastic plastic model

When the stress applied to the model was less than the soil yield strength, the two-element nonlinear viscoplastic model would not be triggered. At this time, the model was still Burgers model, and the constitutive equation was as follows:

$$\varepsilon = \frac{\sigma}{E_1} + \frac{\sigma}{\eta_1}t + \frac{\sigma}{E_2}(1 - \mathrm{e}^{-\frac{E_2}{\eta_2}t}) \tag{6}$$

When the stress applied to the model was greater than the soil yield strength, the model was a six-element nonlinear viscoelastic-plastic creep model. All elements in the model participated in deformation, and the relationship between stress and strain meet the following equations. The constitutive equation was as follows:

$$\eta_1\frac{\mathrm{d}\varepsilon}{\mathrm{d}t} + \frac{\eta_1\eta_2}{E_2}\frac{\mathrm{d}^2\varepsilon}{\mathrm{d}t^2} = \sigma + \left(\frac{\eta_1}{E_2} + \frac{\eta_1+\eta_2}{E_2} + \frac{\eta_1}{\eta_0}t^{\mathrm{n}} + \frac{2\eta_1\eta_2 n t^{\mathrm{n-1}}}{E_2\eta_0}\right)\frac{\mathrm{d}\sigma}{\mathrm{d}t} + \left(\frac{\eta_1\eta_2}{E_2E_2} + \frac{\eta_1\eta_2}{E_2\eta_0}t^{\mathrm{n}}\right)\frac{\mathrm{d}^2\sigma}{\mathrm{d}t^2} + \frac{(\sigma-\sigma_s)\eta_1 n t^{\mathrm{n-2}}}{\eta_0}\left(t + \eta_2\frac{\mathrm{n-1}}{E_2}\right) \tag{7}$$

The creep equation (8) of the soil nonlinear viscoelastic-plastic model could be obtained by Laplace transform and inverse Laplace transform of equation (7).

$$\varepsilon = \frac{\sigma}{E_1} + \frac{\sigma}{\eta_1}t + \frac{\sigma}{E_2}(1 - \mathrm{e}^{-\frac{E_2}{\eta_2}t}) + \frac{\sigma-\sigma_s}{\eta_0}t^n \tag{8}$$

Parameter identification and property analysis

Creep compliance of nonlinear viscoplastic model

When the viscoelasticity of materials was described by creep model, the creep compliance J(t) was usually used to represent the creep energy of materials. It represented the creep strain of materials under unit stress (*Chen et al., 2021*). Its general expression was:

$$J(t) = \varepsilon(t)/\sigma = J_{\mathrm{e}} + J_{\mathrm{v}}(t) + J_{\mathrm{ve}}(t) + J_{\mathrm{vs}}(t) \tag{9}$$

The creep compliance composition of the nonlinear viscoelastic-plastic model was derived. Where J_e stands for elastic compliance; $J_e = 1/E_1$; $J_v(t)$ represents viscosity compliance; $J_v(t) = t/\eta_1$; $J_{ve}(t)$ represents the viscoelastic compliance; $J_{ve}(t) = [1-\exp(-E_2t/\eta_2)]/E_2$; $J_{vs}(t)$ represents the viscoplastic compliance; $J_{vs}(t) = (\sigma-\sigma_s)t^n/\sigma\eta_2$. σ is the applied stress on the material, and t was time of applied stress. According to the expression of creep compliance $J(t)$, the elastic compliance J_e is the instantaneous elastic deformation under the stress applied to paddy soil, which does not change with time. The coefficient of viscosity compliance $J_v(t)$, which increases slowly and linearly with time, is the reciprocal of the coefficient viscosity η_1, where the creep curve shows the creep rate of uniform creep stage of the soil. The viscoelastic compliance $J_{ve}(t)$ is influenced by the delay elastic modulus E_2 and delay viscosity coefficient η_2. As time increases, the viscoelastic compliance $J_{ve}(t)$ gradually increases, then the growth rate slows down to a fixed value. The creep curve illustrates the attenuation creep stage of paddy soil. The viscoplastic compliance $J_{vs}(t)$ represented the viscoplastic strain of soil under unit stress.

Due to the above analysis and equation (8), the fitting of soil nonlinear viscoelastic-plastic model was realized by MATLAB software. The parameters of creep model can be obtained by the fitting equation 8 (Table 3). The determination coefficients of the fitted equations were greater than 0.985, and the coefficient of variation was less than 0.011. The nonlinear viscoelastic-plastic creep model deduced in this study could accurately describe creep properties of paddy soil under multi stress environment.

Table 3

Fitting parameters of soil creep model

Number	**Instant elastic modulus** E_1 [MPa]	**Viscosity coefficient** η_1 [MPa·s]	**Delay elastic modulus** E_2 [MPa]	**Delay viscosity coefficient** η_2 [MPa·s]	η_0 [MPa·s]	R^2
*w*1015	0.243	2062.121	0.814	1.244	/	0.992
*w*1030	0.364	1881.246	0.836	0.915	/	0.984
*w*2045	0.384	1059.369	0.633	0.635	/	0.975
*w*1060	0.398	1203.460	0.789	0.821	/	0.963
*w*1075	0.486	109140.518	4.984	9.758	0.249	0.986
*w*2015	0.424	6724.684	3.450	14.898	/	0.995
*w*2030	0.808	7951.356	3.192	6.958	/	0.992
*w*2045	0.720	4253.545	1.791	2.453	/	0.984
*w*2060	0.579	3837.472	1.517	5.780	/	0.983
*w*2075	0.719	8719737.382	2.336	3.240	0.130	0.997

As shown in Table 3, when the stress level increased from 15% to 75%, the instantaneous elastic modulus and delay elastic modulus of w_1 paddy soil ranged 0.243 - 0.486 MPa and 0.633 - 4.984 MPa with average values of 0.375 and 1.611 MPa, respectively. For w_2 paddy soil, the instantaneous elastic modulus and delay elastic modulus ranged 0.424 - 0.808 MPa and 1.517 to 3.450 MPa with average values of 0.650 MPa and 2.457 MPa, respectively. The paddy soil will produce instantaneous elastic deformation at the moment of loading. The instantaneous elastic modulus and delay elastic modulus represent the elastic mechanical properties of paddy soil. The instantaneous elastic modulus represents the ability of soil to resist instantaneous deformation. The delay elastic modulus stands for the slow degree of elastic change of paddy soil in the stable creep stage. The above analysis showed that in the internal structure of w_1 paddy soil and w_2 paddy soil, the elastic deformation resistance of the spring element E_1 in Maxwell model was less than that of spring element E_2 in the Kelvin model.

The viscosity coefficient represents the fluidity of paddy soil. A larger value indicates a stronger anti-deformation viscosity resistance and poor fluidity. For w_1 paddy soil, the viscosity coefficient and delayed viscosity coefficient ranged 1059.369-109140.518 MPa·s and 0.635-9.758MPa·s with average values of 23069.343 MPa·s and 2.675 MPa·s, respectively. In comparison, w_2 paddy soil exhibited a viscosity coefficient of 3837.472-9414.022 MPa·s (average of 1748500.888MPa·s) and delayed viscosity coefficient of 1.369-4.318 MPa·s (average of 2.613 MPa·s). The above results showed that the viscous resistance to deformation of the viscous element η_1 in Maxwell model was stronger than the delayed viscous element η_2 in the Kelvin model.

Analysis of creep deformation process

By fitting the creep test data according to equations (8), the variation laws of strain, strain rate and strain acceleration during creep deformation could be obtained. The results were shown in Table 4.

Table 4

Fitting equation of soil creep model

Strain fitting	**Strain rate fitting**	**Strain acceleration fitting**
$\varepsilon_1=0.066+7.759\times10^{-6}t+0.020\times(1-e^{-0.654t})$	$v_1=7.759\times10^{-6}+0.013e^{-0.654t}$	$a_1=0.013e^{-0.654t}$
$\varepsilon_2=0.088+1.701\times10^{-5}t+0.038\times(1-e^{-0.913t})$	$v_2=1.701\times10^{-5}+0.035e^{-0.913t}$	$a_2=0.035e^{-0.913t}$
$\varepsilon_3=0.125+4.531\times10^{-5}t+0.076\times(1-e^{-0.996t})$	$v_3=4.531\times10^{-5}+0.076e^{-0.996t}$	$a_3=0.076e^{-0.996t}$
$\varepsilon_4=0.161+5.318\times10^{-5}t+0.081\times(1-e^{-0.962t})$	$v_4=5.318\times10^{-5}+0.078e^{-0.962t}$	$a_4=0.078e^{-0.962t}$
$\varepsilon_5=0.165+7.330\times10^{-7}t+0.016\times(1-e^{-0.511t})+0.040t^{0.201}$	$v_5=7.330\times10^{-7}+8.176\times10^{-3}e^{-0.511t}+8.040\times10^{-3}t^{-0.799}$	$a_5=-4.178\times10^{-3}e^{-0.511t}-6.424\times10^{-3}t^{-1.799}$
$\varepsilon_6=0.040+2.528\times10^{-6}t+0.005\times(1-e^{-0.232t})$	$v_6=2.528\times10^{-6}+1.160\times10^{-3}e^{-0.232t}$	$a_6=1.160\times10^{-3}e^{-0.232t}$
$\varepsilon_7=0.042+4.276\times10^{-6}t+0.011\times(1-e^{-0.459t})$	$v_7=4.276\times10^{-6}+5.049\times10^{-3}e^{-0.459t}$	$a_7=5.049\times10^{-3}e^{-0.459t}$
$\varepsilon_8=0.071+1.199\times10^{-5}t+0.028\times(1-e^{-0.730t})$	$v_8=1.199\times10^{-5}+0.020e^{-0.730t}$	$a_8=0.020e^{-0.730t}$
$\varepsilon_9=0.117+1.772\times10^{-5}t+0.045\times(1-e^{-0.263t})$	$v_9=1.772\times10^{-5}+0.012e^{-0.263t}$	$a_9=0.012e^{-0.263t}$
$\varepsilon_{10}=0.118+9.748\times10^{-9}t+0.036\times(1-e^{-0.721t})+0.039t^{0.136}$	$v_{10}=9.748\times10^{-9}+0.026e^{-0.721t}+5.304\times10^{-3}t^{-0.864}$	$a_{10}=0.019e^{-0.721t}-4.583\times10^{-3}t^{1.864}$

ε_1 - ε_{10}, v_1-v_{10} and a_1-a_{10} were the corresponding strain, strain rate and strain acceleration of *w*1015 - *w*2075 samples respectively. It could be seen that when the stress level was below 75%, the total creep deformation of the two groups of paddy soil was composed of elastic strain $\varepsilon_e(t)$, viscous strain $\varepsilon_v(t)$ and viscoelastic strain $\varepsilon_{ve}(t)$. When the load at 75% stress level was applied, the total strain of paddy soil included viscoplastic strain $\varepsilon_{vs}(t)$ in addition to the above three strains.

The proportion of each strain in the total strain was further analysed using the following formula.

$$P_i(t)=\frac{\varepsilon_i(t)}{\varepsilon(t)}\times 100\%=\frac{J_i(t)}{J_e(t)+J_v(t)+J_{ve}(t)+J_{vs}(t)}\times 100\% \quad (10)$$

Fig. 5 showed the variation law of strain proportion with time under unit stress. The proportion of elastic strain in total strain (P_e) decreased nonlinearly with time. The proportion of viscous strain to total strain (P_v) increased with creep time. The proportion of viscoelastic strain in the total strain (P_{ve}) first increased and then decreased with time. The elastic strain increased with the increase of stress level. When the applied stress did not reach the yield strength, the variation trend of viscosity and viscoelastic strain was the same as that of elastic strain. When the stress exceeded the yield strength, an opposite trend can be observed for the viscous and viscoelastic strain. When the stress level increased from 10% to 45%, the proportion of elastic strain (P_e) decreased with it; the viscous and viscoelastic strains (P_v and P_{ve}) increased with it. When the stress level increased from 45% to 60%, this law of change was opposite to the previous one. Under each stress level, the smallest proportion of each strain was viscous strain. When the stress level increased to 75%, the proportion of viscous strain would decrease sharply. The reason was that its proportion was replaced by the viscoplastic strain. The general trend of strain and proportion of w_1 soil and w_2 soil with time and stress level was the same, which did not change with the varying of soil moisture content.

The proportion of each strain in the steady state strain of soil **Table 5**

Number	ε_1	ε_2	ε_3	ε_4	ε_5	ε_6	ε_7	ε_8	ε_9	ε_{10}
ε_e [%]	6.60	8.80	12.50	16.10	16.50	4.00	4.20	7.10	11.70	11.80
ε_v [%]	0.70	1.53	4.08	4.79	0.07	0.02	0.04	1.08	1.59	8.77×10^{-4}
ε_{ve} [%]	2.00	3.80	7.60	8.10	1.60	0.05	1.10	2.80	4.50	3.60
ε_s [%]	/	/	/	/	15.70	/	/	/	/	9.84
P_e [%]	70.98	62.27	51.70	55.54	48.72	84.61	73.88	64.67	65.75	46.76
P_v [%]	7.51	10.83	16.87	16.51	0.19	4.81	6.77	9.83	8.96	3.48×10^{-3}
P_{ve} [%]	21.51	26.89	31.43	27.94	4.72	10.58	19.35	25.50	25.29	14.26
P_{vs} [%]	/	/	/	/	46.36	/	/	/	/	38.98

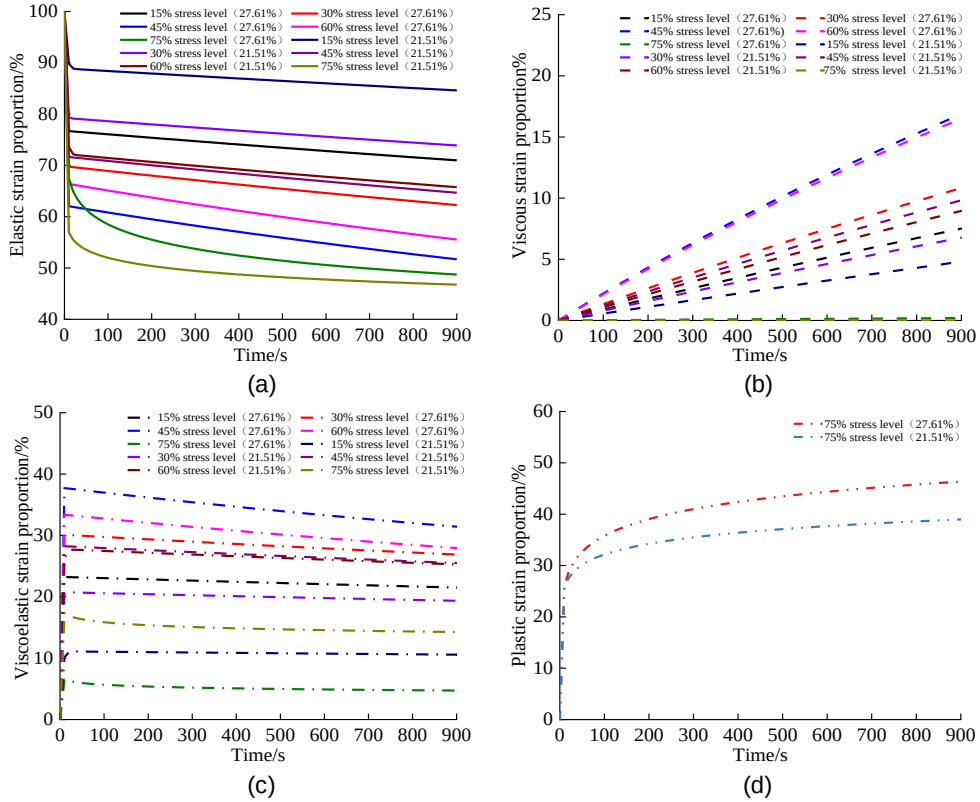

Fig. 5 - The curve of strain proportion with time

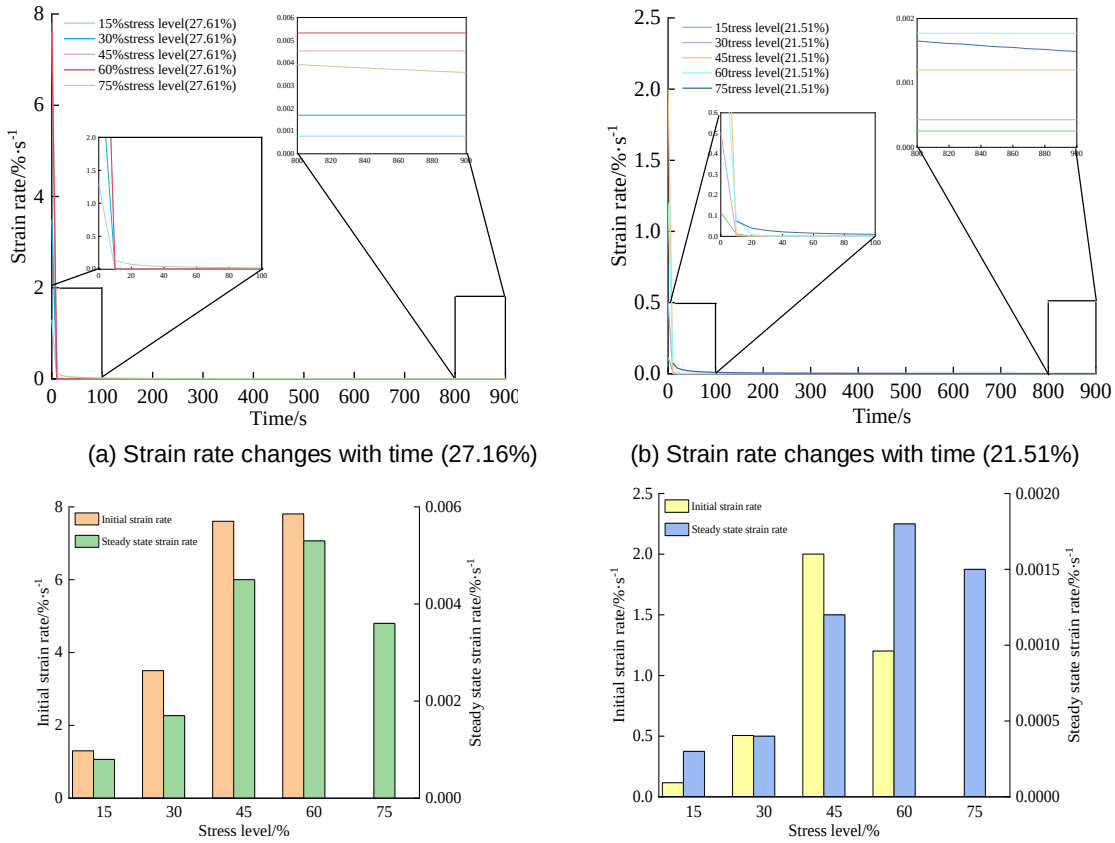

(a) Strain rate changes with time (27.16%)

(b) Strain rate changes with time (21.51%)

(c) The initial rate and steady-state strain rate (27.16%)

(d) The initial rate and steady-state strain rate (21.51%)

Fig. 6 - Soil creep rate under different stresses

When the applied stress was less than the yield strength, the strain rate of paddy soil was composed of viscous strain rate and viscoelastic strain rate. After the applied stress exceeded the yield strength, the strain rate included viscoplastic strain rate in addition to the above two rates (Fig. 6). In the creep process, all samples show obvious differences in the initial stage. According to Table 4 and equation (8), when $0 < n < 1$, the creep rate was greater than 0 and the creep acceleration was less than 0. The paddy soil at each stress level showed instantaneous creep stage, attenuation creep stage and steady state creep stage in the process of compression creep. Due to the mathematical definition of strain expression at 75% stress level, the initial strain rate cannot be deduced according to the formula. Therefore, the steady state strain rates of *w*1015, *w*1030, *w*1045, *w*1060 and *w*1075 were 0.0008, 0.0017, 0.0045, 0.0053 and 0.0351%·s^{-1} respectively, with initial strain rates of 1.3008, 3.5017, 7.6045 and 7.8053%·s^{-1}. The steady state strain rates corresponding to *w*2015, *w*2030, *w*2045, *w*2060 and *w*2075 were 0.003, 0.0004, 0.0012, 0.0018 and 0.0015 %·s^{-1} respectively, with initial strain rates of 0.1163, 0.5053, 2.0012 and 1.2018%·s^{-1}.

Creep model verification

According to the creep constitutive equations of the two models, the difference of the models would be reflected when the loading stress was above the yield strength. Therefore, based on the above experimental method, the soil of the same paddy field was taken again. The measured moisture content was 19.65%, and the compressive strength was 0.136 MPa. The 75% stress level creep test was carried out on the soil, and the creep steady stage strain was 22.699%. The derived nonlinear creep model and Burgers model were used to fit and analyse the creep test data respectively (Fig. 7).

The determination coefficients of the fitting equations of the nonlinear viscoelastic-plastic model and the Burgers model were 0.997 and 0.989 (Table 5). The variation law of the nonlinear viscoelastic-plastic model was generally consistent with the creep test curve, and the model exhibited better regularity and accuracy than Burgers model. Although the fitting accuracy between Burgers model and creep test value was good in the initial creep stage, it was because the nonlinear viscoelastic-plastic model introduced viscoplastic deformation, resulting in the small instantaneous strain of the initial creep stage.

However, with the extension of creep time, the fitting effect between nonlinear viscoelastic-plastic model and creep test data was obviously better than Burgers model. Especially in the steady state creep stage, the difference was more obvious. The creep steady state strains of nonlinear model and Burgers model were 22.796% and 22.887% respectively, with the relative errors of 0.437% and 0.827%. The creep curve predicted by Burgers model showed a linear growth trend in the later stage of creep, which deviated from the creep test curve. The result was consistent with the above theoretical analysis. In conclusion, the nonlinear viscoelastic-plastic creep model established in our study was scientific and reasonable, and could more accurately reflect the whole creep process of paddy soil.

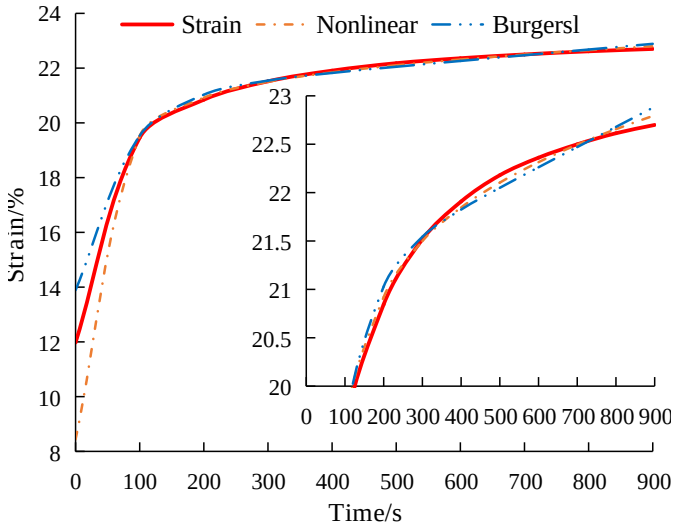

Fig. 7 - Comparison of fitting result

Table 5

The proportion of each strain in the steady state strain of soil

Model	Steady stage strain [%]	E_1 [MPa]	η_1 [MPa·s]	E_2 [MPa]	η_2 [MPa·s]	η_0 / [MPa·s]	Relative error [%]	R^2
Nonlinear	22.799	0.142	1111111.111	0.276	17.922	0.046	0.437	0.997
Burgers	22.887	0.734	4899.135	1.432	99.553	/	0.827	0.989

CONCLUSIONS

(1) The compression creep properties of paddy soil were analysed, and a two-element nonlinear viscoplastic model modified by power function was established. By connecting the nonlinear viscoplastic model with Burgers model in series, a six-element creep model which could fully reflect the nonlinear viscoelastoplastic creep properties of paddy soil was derived.

(2) According to the test data, the parameters of the nonlinear viscoelastoplastic model were identified, and the fitting determination coefficients of creep curves at each stress level were more than 0.96. The creep curves of paddy soil with moisture content of 19.65% were compared and predicted at 75% stress level. The determination coefficient and relative error were 0.997% and 0.437% respectively. It showed that the model was feasible to predict the creep properties and deformation behaviour of paddy soil.

(3) The creep process was the transition of the internal structure of paddy soil from unbalanced state to equilibrium state after applied stress. The time when the deformation reached the steady state was mainly affected by the viscosity, elasticity, plasticity and their coupling effects in the soil. When the damage caused by the force applied to the soil accumulates to a certain extent, the soil will be destroyed.

ACKNOWLEDGEMENT

This study was financially supported by a program of China's National Natural Science Foundation Project (No. 31901412), the National Key Technology R&D Programme (No. 2017YFD0301300) and the Special Fund for Agro-scientific Research in the Public Interest (No. 201503136).

REFERENCES

[1] Vaitauskien K., Arauskis E., Romaneckas K. et al., (2017), Design, development and field evaluation of row-cleaners for strip tillage in conservation farming. *Soil &Tillage Research*, vol. 174, pp. 139-146.

[2] Schmalz H., Taylor R., Johnson T. et al., (2013), Soil morphologic properties and cattle stocking rate affect dynamic soil properties. *Rangeland Ecology & Management*, vol. 66, pp. 445-453.

[3] Zeng Z., Chen Y., Zhang X., (2017), Modelling the interaction of a deep tillage tool with heterogeneous soil. *Computers and Electronics in Agriculture*, vol. 143, pp. 130-138.

[4] Wang X., Zhang S., Pan H. et al., (2019), Effect of soil particle size on soil-subsoiler interactions using the discrete element method simulations. *Biosystems Engineering*, vol. 182, pp. 138-150.

[5] Kong F., Wu T., Chen C. et al., (2021), Mechanical properties and construction of constitutive model for compression and stress relaxation of seed cotton (*籽棉压缩与应力松弛力学特性及模型构建*). *Transactions of the Chinese Society of Agricultural Engineering*, vol. 37, Issue 7, pp. 53-60.

[6] Wang, P, Liu, E., Song, B. et al., (2019). Binary medium creep constitutive model for frozen soils based on homogenization theory. *Cold Regions Science and Technology*, vol.162, pp. 35-42.

[7] Engelund E., Salmen L. (2012), Tensile creep and recovery of Norway spruce influenced by temperature and moisture. *Holzforschung*, vol. 66, pp. 959-965.

[8] Xiang, G., Yin, D., Cao, C. et al., (2021), Creep modelling of soft soil based on the fractional flow rule: simulation and parameter study. *Applied Mathematics and Computation*, vol. 403. https://doi.org/10.1016/j.amc.2021.126190.

[9] Zheng K. (2019), Research status and prospect of soil anti-adhesion technology for tillage equipment. (*耕整机械土壤减粘脱附技术研究现状与展望*). *Journal of Anhui Agricultural University*, vol. 46, Issue 4, pp. 728-736.

[10] Zhu Y., Xia J., Zeng R. et al., (2020), Prediction Model of Rotary Tillage Power Consumption in Paddy Stubble Field Based on Discrete Element Method (*基于离散元的稻板田旋耕功耗预测模型研究*). *Transactions of the Chinese Society for Agricultural Machinery*, vol. 51, Issue 10, pp. 42-50.

[11] Zhu Y., Zhang J., Zeng R. et al., (2019), Design and experiment of herringbone type rotary blade roller for burying stubble in paddy field and dry land (*人字型水旱两用旋埋刀辊设计与试验*). *Transactions of the Chinese Society for Agricultural Machinery*, vol. 50, Issue 4, pp. 49 - 57.

[12] Zou L., Wang S., Lai X., (2013), Creep model for unsaturated soils in sliding zone of Qianjiangping landslide. *Journal of Rock Mechanics and Geotechnical Engineerin*g, vol. 5, Issue 2, pp. 162-167.

[13] Aleksandar S., Okuka., Dušan Z., (2020), Fractional Burgers models in creep and stress relaxation tests. *Applied Mathematical Modelling*, vol. 77, Issue 2, pp. 1894-1935.

[14] Liu J., Bai X., Li P., (2013), Modified Burger's model for describing creep behaviour of tomato fruits (番茄果实蠕变特性表征的 Burger's 修正模型). *Transactions of the Chinese Society of Agricultural Engineering*, vol. 29, Issue 9, pp. 249-255.

[15] Chen S., Wei Y., Zhao K. et al., (2021), Creep performance and prediction model of bamboo scrimber under compression (*重组竹顺纹受压蠕变性能及预测模型*). *Acta Materiae Compositae Sinica*, vol. 38, Issue 3, pp. 44-952.